arXiv:1210.5602v1 [cond-mat.mtrl-sci] 20 Oct 2012

Stabilizing intrinsic defects in SnO_2

Gul Rahman* and Naseem Ud Din
Department of Physics, Quaid-i-Azam University, Islamabad 45320, Pakistan

Víctor M. García-Suárez
Departamento de Física, Universidad de Oviedo, 33007 Oviedo Spain
Nanomaterials and Nanotechnology Research Center (CINN), CSIC - Universidad de Oviedo, Spain and
Department of Physics, Lancaster University, Lancaster LA1 4YW, United Kingdom
(Dated: October 23, 2012)

The magnetism and electronic structure of Li-doped SnO_2 are investigated using first-principles LDA calculations. We find that Li induces magnetism in SnO_2 when doped at the Sn site but becomes non-magnetic when doped at the O and interstitial sites. The calculated formation energies show that Li prefers the Sn site, in agreement with previous experimental works. The interaction of Li with native defects (Sn V_{Sn} and O V_O vacancies) is also studied, and we find that Li not only behaves as a spin polarizer, but also a vacancy stabilizer, i.e. Li significantly reduces the defect formation energies of the native defects and helps the stabilization of magnetic oxygen vacancies. The electronic densities of states reveal that those systems, where the Fermi levels touch the conduction (valence) band, are non-magnetic (magnetic).

PACS numbers: 71.22.+i, 71.55.-i, 75.75.Pp, 61.72.jd, 61.72.jj

I. INTRODUCTION

Diluted magnetic semiconductors (DMS) have recently been a major focus of magnetic semiconductor research. In the recent past, ferromagnetism (FM) above room temperature have been extensively investigated in transition metal (TM)-doped wide band gap oxide semiconductors, e.g. ZnO[1,2] and TiO_2 [3–5]. Among these wide band gap semiconductors SnO_2 has long been a material of interest for applied and pure research purposes. In 2002, Ogale *et al.*[6] not only reported room temperature FM in Co-doped SnO_2, but also very large magnetic moments. Later on density functional theory (DFT) calculations showed that Sn vacancies, V_{Sn}, can induce magnetism in SnO_2 and he observed large magnetic moment was attributed to its influence.[7] Recently, several experimental and theoretical reports showed that cation vacancies can induce magnetism not only in SnO_2, but also in ZnO, TiO_2, ZrO_2, In_2O_3,CeO_2 HfO_2[8–13].

Following the prediction of magnetism without TM impurities, much interest was also diverted to magnetism induced by light element doping in host semiconductor matrices, e.g., K, N, Mg, and C-doped SnO_2 [14–18]. There are experimental evidences which clearly demonstrate room temperature FM induced by light elements.[19,20] However, the exact nature of magnetism in these semiconductor oxides is still under debate. Recent experimental reports claim that pristine SnO_2 nanocrystalline thin films exhibit room temperature FM, but the magnetic moment is suppressed when doped with Gd.[21] The presence of large amounts of singly ionized oxygen vacancies (V_O^+), rather than V_{Sn} or V_O were found to be responsible for the observed FM in pristine SnO_2 thin films.[21] On the other hand Chang et al.[22] observed FM in very thin pristine SnO_2 films which was induced by the presence of oxygen vacancies located near the film surface. There is also a belief that the observed FM in undoped SnO_2 mainly originates from the bulk double oxygen vacancies.[23] In contrast Wang et al.[24] studied nanosheets of SnO_2 and they found that the saturation magnetization of all their annealed samples did not feature mono-dependence on oxygen vacancies, whereas an Sn vacancy related origin was accounted for variations in the magnetization of their studied samples.

Light elements can induce magnetism, but the observed magnetism has also a linkage with native defects. However, whether magnetism is induced by cation or anion vacancies in the pristine host material or doped with light elements, the defect formation energies of native defects, which are important for magnetism, are very high. Oxygen vacancies rather than tin vacancies are considered as a source of magnetism due to its lower formation energy,[25] but neutral V_O does not induce magnetism in oxides.[7,20,26] The major issue in magnetism induced by vacancies is therefore that these magnetic systems have high formation energies [27,28]. Consequently, to realize defects-driven magnetism experimentally it is essential to reduce the defect formation energy of the host material (SnO_2 in our case). We choose Li as a dopant[29] that can modify the defect formation energies of native defects in SnO_2. We show that Li can indeed significantly reduce the formation energies of various types of defects. This is, as far as we know, the first theoretical study performed on the interaction of Li with native defects in SnO_2.

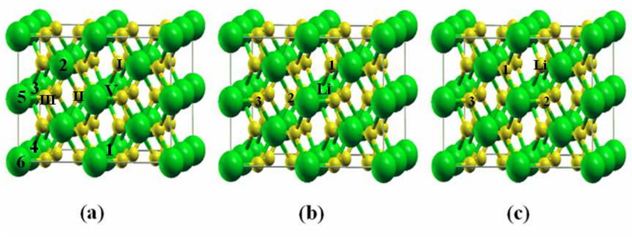

FIG. 1: (color online) A $2 \times 2 \times 2$ supercell of SnO_2. In (a) V represents the Sn vacancy, which is fixed at the center of the supercell. The positions of Li doped at different Sn sites are marked as 1-6, whereas the positions of Li doped at O sites are shown by I,II, and III. In model (b) the central atom represents the Li atom doped at the Sn site and the O vacancies are marked as 1-4. In model (c) Li is doped at the O site, marked as Li, and the oxygen vacancies are created at the oxygen sites marked as 1, 2, and 3. Big (green) and small (blue) balls represent Sn and O atoms, respectively.

II. COMPUTATIONAL MODELS AND METHOD

SnO_2 is known to crystallize in the rutile structure with space group $P4_2/mnm$ or D_{14}^{4h} (SG136) under ambient conditions.[30] We used our previously optimized lattice parameters.[7] To simulate the defects a $2 \times 2 \times 2$ supercell of SnO_2 containing 48 atoms was employed. We considered the following models to investigate the detailed energetics and magnetic properties of different defects in SnO_2.

a) Li-doped SnO_2: Li was doped at the Sn, O, and interstitial sites, denoted as Li_{Sn}, Li_O, and Li_{int}, respectively.

b) V_{Sn}+ Li_{Snj}:In this case, V_{Sn} was fixed at the center of the supercell, and Li was doped at different Sn j sites, with $j = 1 - 6$ (see Fig. 1(a)).

c) V_{Sn}+ Li_{Oj}: In this case, V_{Sn} was fixed at the center of the supercell, and Li was doped at different O j sites, with j=I, II, III (see Fig. 1(a)).

d) V_{Sn}+ Li_{int}: Here V_{Sn} was fixed at the center of the supercell and Li was doped at interstitial sites.

e) V_{Oj}+ Li_{Sn}: Here Li was doped at the central Sn site and V_O was created at different O j sites, with $j = 1 - 4$ (see Fig. 1(b))

f) V_O+ Li_{Oj}: In this case, V_O was fixed and Li was doped at different O j sites, with $j = 1, 2, 3$ (see Fig. 1(c))

g) V_O+ Li_{int}: Here V_O was fixed at the center of the supercell and Li was doped at interstitial sites.

We performed calculations in the framework of density functional theory (DFT) [31] using linear combination of atomic orbitals (LCAO) as implemented in the SIESTA code [32]. The local density approximation (LDA)[33] was adopted for describing exchange-correlation interactions. We used standard norm-conserving pseudopotentials [34] in their fully nonlocal form [35]. Atomic positions and lattice parameters were optimized, using a conjugate-gradient algorithm [36], until the residual Hellmann-Feynman forces converged to less than 0.05 eV/Å. A cutoff energy of 400 Ry for the real-space grid was adopted.

The concentration of dopants and vacancies in a crystal depends upon its formation energies (E_f). The chemical potentials, which vary between the stoichiometric and diluted limits, depend on the material growth conditions and boundary conditions. We have calculated the formation energies under equilibrium conditions, O-rich conditions and Sn-rich conditions. Under equilibrium conditions, for SnO_2 the chemical potentials of O and Sn satisfy the relationship $\mu_{Sn} + 2\mu_O = \mu_{SnO_2}$, where μ_{SnO_2}, the chemical potential of bulk SnO_2, is a constant value calculated as the total energy per SnO_2 unit formula [37]. Under Sn rich conditions, μ_{Sn}=E(Sn^{metal}), $\mu_O = \left(\frac{\mu_{SnO2} - \mu_{Sn}}{2}\right)$. O rich condition gives $\mu_O = \left(\frac{1}{2}\right)$E($O_2$), $\mu_{Sn} = \mu_{SnO2} - 2\mu_O$.

The formation energies for systems with intrinsic defects, either Sn or O vacancies, can be calculated in the following way:

$$\mathrm{E_f} = \mathrm{E^d} - \mathrm{E^p} + n\mu_X, \qquad (1)$$

where μ_X is chemical potential of X (X = Sn, O), n is the number of atoms removed from the system and E^d and E^p are the total energies of the defected and the pure system, respectively.

The formation energy of the Li doped system can be calculated as

$$\mathrm{E_f} = \frac{1}{n}\left(\mathrm{E^d} - \mathrm{E^p} + n\mu_X - m\mu_{Li}\right), \qquad (2)$$

where μ_{Li} is the chemical potential of bulk lithium, calculated as total the energy per unit cell of bulk Li, n is number of atoms removed and m is number of atoms added to the system.

III. RESULTS AND DISCUSSIONS

In this section, we will discuss our DFT results. We will focus on Li-doped SnO_2 systems, and then we will move to discuss the interactions of Sn and O vacancies with Li.

TABLE I: Formation energies calculated under equilibrium (E_{eq}), Sn-rich (E_{Sn}) and O-rich (E_{O}) conditions, in units (eV). The last column lists magnetic moments (MM) per supercell , calculated in units of μ_{B}. Values in brackets show formation energies of the unrelaxed structures.

System	E_{eq}	E_{Sn}	E_{O}	MM
$\mathrm{Li_{Sn}}$	-1.03(-0.89)	6.53 (6.67)	-1.03(-0.89)	3.00
$\mathrm{Li_{O}}$	-0.85 (5.72)	-0.85 (5.72)	2.93 (9.50)	0.00
$\mathrm{Li_{int}}$	-2.58(-1.63)	-2.58(-1.63)	-2.58(-1.64)	0.00
$\mathrm{V_{Sn}}$	6.87 (7.32)	14.44(14.88)	6.87 (7.32)	4.00
$\mathrm{V_{O}}$	1.64 (1.69)	1.64 (1.69)	5.42 (5.47)	0.00

A. Li-doped $\mathrm{SnO_2}$

First, we calculate, using the above equations, the defect formation energies of the doped $\mathrm{SnO_2}$ systems, where Li was doped at the Sn, O, and interstitial sites, as stated before. The calculations (see Table (I)) show that the doping of Li at the Sn site has the lowest formation energy (-1.03 eV) under stoichiometric and O-rich conditions. For comparison purposes, the formation energies of unrelaxed systems are also given in Table (I). It is clear that the structural relaxation is not very effective when Li is doped at the Sn site. This behavior can easily be understood in terms of the atomic sizes of the Sn and Li atoms. The atomic radii of Sn and Li are 1.41 Åand 1.45 Å, respectively. The doped Li is surrounded by six O atoms and the optimized bond lengths between them (LiO distances) have two different values, 1.97 Å, and 2.03 Å, which are comparable to the pure bond lengths of SnO in $\mathrm{SnO_2}$, i.e., 2.04 Å and 2.08Å. Since both Li and Sn approximately have the same atomic radius, then Li at the Sn site will not distort the structure and it is expected that the Sn site will be favorable for Li. Indeed our calculations also show that Li at the Sn site has the lowest formation energy, which agrees with experimental observations[29]. On the other hand, Li at the O site has a larger formation energy under the equilibrium condition. One can also see that the formation energy of Li at the O site is very large when structural relaxation is not allowed but decreases significantly when structural relaxation is permitted, which is followed by a large structural distortion. Our structural analysis shows that when Li is doped at the O site, it goes to interstitial site and leaves behind an O vacancy. So, it indicates that the formation energy of O is lowered mainly due to a structural deformation which is accompanied by the movement of Li to an interstitial position. At the same time, the system remains nonmagnetic. To be more confident, we also carried out separate calculations on Li at interstitial sites with and without O vacancies, and we got the same conclusion, which will be discussed below. Indeed, interstitial Li has the lowest formation energy, but it does not induce magnetism in $\mathrm{SnO_2}$, so we will not focus on it.

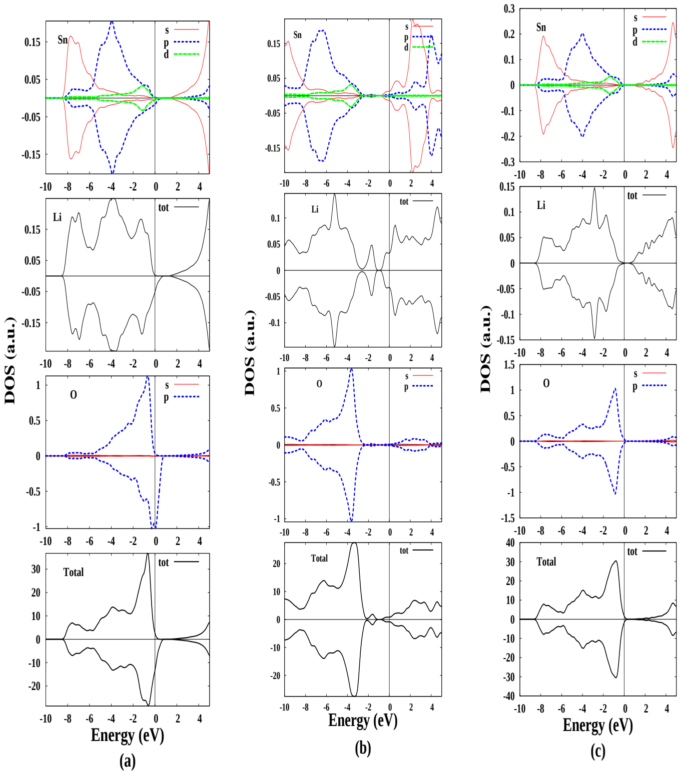

FIG. 2: (color online)The calculated total and partial density of states (DOS) of (a) $\mathrm{Li_{Sn}}$, (b) $\mathrm{Li_{O}}$, and (c) $\mathrm{Li_{int}}$ systems. Solid (red) and dashed (blue, green) lines represent *s* and *p*, *d* states, respectively. In the bottom panels the solid line represents the total DOS. The positive (negative) DOS shows majority (minority) spin states. The Fermi level (E_{F}) is set to zero.

As stated above, doped Li prefers the Sn site under stoichiometric and O-rich conditions and has large magnetic moment (3.00 μ_{B}). Since the nominal valence of Sn in a perfect $\mathrm{SnO_2}$ is $\mathrm{Sn^{4+}}$, and Li is a cation with valence of $\mathrm{Li^{1+}}$,[29] when Li is doped at Sn site in pure $\mathrm{SnO_2}$, it donates one electron to compensate one hole among the four holes generated by the Sn deficiency. The three uncompensated holes, localized at the O sites, give a magnetic moment of 3.00 μ_{B} per supercell. To see the atomic origin of magnetism in Li-doped $\mathrm{SnO_2}$, we calculated the total and atom projected partial density of states(PDOS) of the Sn, O, and Li atoms (see Fig. 2). The substitutional Li impurity polarizes the host band which gives rise to a induced impurity peak close to the valance band edge in the spin-down part of the total DOS, while the spin-up part is influenced slightly. Such a behavior suggests that Li behaves as a *p* type dopant in $\mathrm{SnO_2}$.[29] The low lying *s* orbitals of Li are spin-polarized and strongly hybridized with the *p* orbitals of O. The Fermi energy is mainly dominated by the *p* orbitals of O, which indicates that magnetism is mainly induced by the *p* orbitals and localized at the O atom. Indeed, the oxygen atoms surrounding the doped Li are the main ones that contribute to magnetism. We also see that the spin down state is partially occupied which contributes to the magnetic moment. The majority s spin states of Li are completely occupied and the minority spin states are partially occupied, leading to a significant spin splitting near the Fermi level.

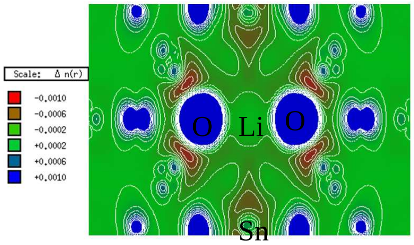

FIG. 3: (color online)Spin density contours for the Li-doped SnO_2 (110) plane. Labels show atomic sites

To further emphasize on the nature of magnetism, the spin density contours are shown in Fig. 3. It is interesting to see that Li polarizes the O and Sn atoms in opposite directions, and the polarization is not only limited to the nearest O atoms surrounding the Li atoms, but it also spreads to other O atoms which are far from Li. It seems that the origin of magnetism in light elements doped-SnO_2 or Sn vacancies in SnO_2 is the same i.e., the surrounding O atoms become polarized. However, the remarkable feature of Li doped SnO_2 is that there is a very small (negligible) induced magnetic moment at the Li site. This behavior is quite different from other light elements doped SnO_2 systems[14–16] which suggests that Li behaves as a spin polarizer in SnO_2. We note that Li doped at O and interstitial sites does not induce magnetism (see Fig. 2). Test calculations on a supercell of 2 × 2 × 3 (containing 72 atoms) were also carried out and we found the same behavior, i.e. Li at the Sn site gives 3.00 μ_B magnetic moment per supercell, whereas Li at the O site does not show any magnetic moment.

TABLE II: Formation energies (in units of eV) of systems V_{Sn} + Li_{Sn}, V_{Sn} + Li_O, and V_{Sn} + Li_{int} calculated under equilibrium (E_{eq}), Sn-rich (E_{Sn}) and O-rich (E_O) conditions. The distance from V_{Sn} to Li_{Sn}, Li_O, and Li_{int} is $r-r_j$ (in units of Å). The last column lists the calculated magnetic moments (MM) per supercell (in units of μ_B). Values in brackets show the formation energies of the unrelaxed structures.

System	$r-r_j$	E_{eq}	E_{Sn}	E_O	MM
V_{Sn}		6.87(7.32)	14.44(14.88)	6.87(7.32)	4.00
V_{Sn} + Li_{Sn_j}					
V_{Sn} + Li_{Sn1}	3.23	1.55(2.19)	9.11(10.39)	1.55(2.83)	7.00
V_{Sn} + Li_{Sn2}	3.76	2.13(2.91)	9.69(10.47)	2.13(2.91)	7.00
V_{Sn} + Li_{Sn3}	4.80	1.54(3.04)	9.10(10.60)	1.54(3.04)	7.00
V_{Sn} + Li_{Sn4}	5.78	1.56(3.02)	9.13(10.59)	1.56(3.02)	7.00
V_{Sn} + Li_{Sn5}	6.79	2.80(3.04)	10.36(10.61)	2.80(3.04)	7.00
V_{Sn} + Li_{Sn6}	7.52	2.91(3.14)	10.48(10.70)	2.91(3.14)	7.00
V_{Sn} + Li_{O_j}					
V_{Sn} + Li_{OI}	2.04	-4.16(4.87)	3.40(12.44)	-0.38(8.65)	1.00
V_{Sn} + Li_{OII}	2.08	-3.74(5.39)	3.82(12.95)	0.04(9.17)	1.00
V_{Sn} + Li_{OIII}	4.71	6.09(10.91)	13.65(18.47)	4.93(14.69)	1.00
V_{Sn} + Li_{int}					
V_{Sn} + Li_{int}	5.73	1.83(4.04)	9.40(11.60)	1.83(4.04)	3.00

B. Interaction of Sn vacancies with Li

We will move now to discuss the interactions of intrinsic defects (Sn and O vacancies) with Li. We found that a single Sn vacancy induces a very large magnetic moment ∼4.00 μ_B which agrees with previous calculations[7]. However, V_{Sn} has a very large formation energy in both the O-rich (6.87 eV) and Sn-rich(14.44 eV) conditions. Structural relaxation does not have a significant effect on the formation energy. To reduce the formation energy of V_{Sn}, which is the core of this article, we considered an Sn vacancy at the center of the supercell, and doped Li at different Sn sites (see Figure 1). The formation energies are given in Table (II). By doping Li at the Sn site, Li significantly reduces the defect formation energy of V_{Sn}. The case V_{Sn}+Li_{Sn3} has the lowest formation energy ∼1.54 eV, which shows that Li doping is much more favorable energetically in SnO_2 than previously reported Zn[27] and Cr[28] doped-SnO_2: The formation energies of the system with Zn_{Sn}+V_{Sn} are 16.50 eV and 7.00 eV under O-poor and the O-rich conditions[27], repectively. Doping Cr in SnO_2 with V_{Sn} produces formation energies ∼12.00 eV and 2.00 eV under O-poor and O-rich conditions[28], respectively. While in our case they are 9.10 eV and 1.54 eV under O-poor and O-rich conditions, respectively. It is interesting to see that Li not only stabilizes V_{Sn}, but also has the largest magnetic moment 7.00 μ_B per supercell. When the Li atom occupies the Sn site, it donates one electron to compensate one hole among the four holes generated by the substituted Sn. These three uncompensated holes along with the four holes of neutral V_{Sn} give a total of 7.00 μ_B magnetic moment per supercell.

Once found that Li at Sn sites significantly reduces the defect formation energy of Sn vacancies, then we doped Li at the O site in the presence of V_{Sn}. In this case, we also fixed V_{Sn} and doped Li at different O sites, mainly considering those O atoms which are near and far from V_{Sn}. The calculated formation energies are shown in Table (II). It is clear that the unrelaxed systems have large positive formation energies (endothermic processes), but after structural relaxation we found negative formation energies (exothermic processes). When Li was doped at O sites around V_{Sn} it goes to an interstitial site (near

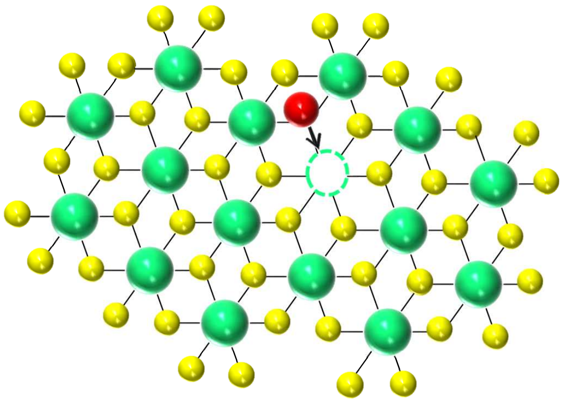

FIG. 4: (color online)Schematic representation of structural relaxations in the $\mathrm{Li_O} + V_{\mathrm{Sn}}$ system. Green, yellow, and red balls represent Sn, O, and Li atoms, respectively. The Sn vacancy (V_{Sn}) is represented by a green dashed circle. The arrow represents movement of the Li atom towards V_{Sn} during structural relaxation.

$\mathrm{V_{Sn}}$) to form a stable structure, after structural relaxation. This process leaves behind an oxygen vacancy and Li interstitial near $\mathrm{V_{Sn}}$ (see Fig. 4). This exothermic process further indicates that doped Li does not prefer the O site, rather it prefers the interstitial site, as stated above. As shown also above, the $\mathrm{Li_O}$ and $\mathrm{Li_{int}}$ systems have no magnetic moment, whereas $\mathrm{V_{Sn}}$ has large magnetic moment. However, when Li is doped at the O site in a system with $\mathrm{V_{Sn}}$, it breaks the bonds with the neighboring Sn atoms and goes to the nearest interstitial site leaving behind an O vacancy. Three out of the four holes generated by $\mathrm{V_{Sn}}$ are compensated by 2^- charge state of $\mathrm{V_O}$ and one electron of Li, leaving behind a single hole that gives a magnetic moment of 1.00 μ_{B}. When Li is far from $\mathrm{V_{Sn}}$ ($\mathrm{V_{Sn}}$+Li_{OIII} case), the Li atom does not form a stable structure.

We discuss now the interaction of Sn vacancies with $\mathrm{Li_{int}}$. In this case, we doped Li at an interstitial site which was 5.37 Å away from $\mathrm{V_{Sn}}$. The defect formation energy of this system is given in Table (II). Although the $\mathrm{Li_{int}}$ + $\mathrm{V_{Sn}}$ system behaves endothermically, the formation energy of $\mathrm{V_{Sn}}$ decreases so much as compared with $\mathrm{V_{Sn}}$ system without $\mathrm{Li_{int}}$. Note that the structural relaxation does not change the sign of E_{f}. The $\mathrm{Li_{int}}$ + $\mathrm{V_{Sn}}$ system also shows a large magnetic moment, 3.00 μ_{B} per supercell, or in other words, when Li is at the interstitial site it interacts with $\mathrm{V_{Sn}}$ and reduces the magnetic moment of $\mathrm{V_{Sn}}$. From the above thermodynamics of different defects in $\mathrm{SnO_2}$, we can conclude that among all these defects the $\mathrm{V_{Sn}}$ + $\mathrm{Li_O}$ complex has the lowest energy. In the presence of vacancies (Sn and O), Li prefers to occupy the O site rather than going into Sn or interstitial sites. Although, interstitial Li also reduces the formation energy of $\mathrm{V_{Sn}}$, it is not a favorable process. Note that different defective systems of Li-doped ZnO showed the same type of behavior in a previously reported work.[20]

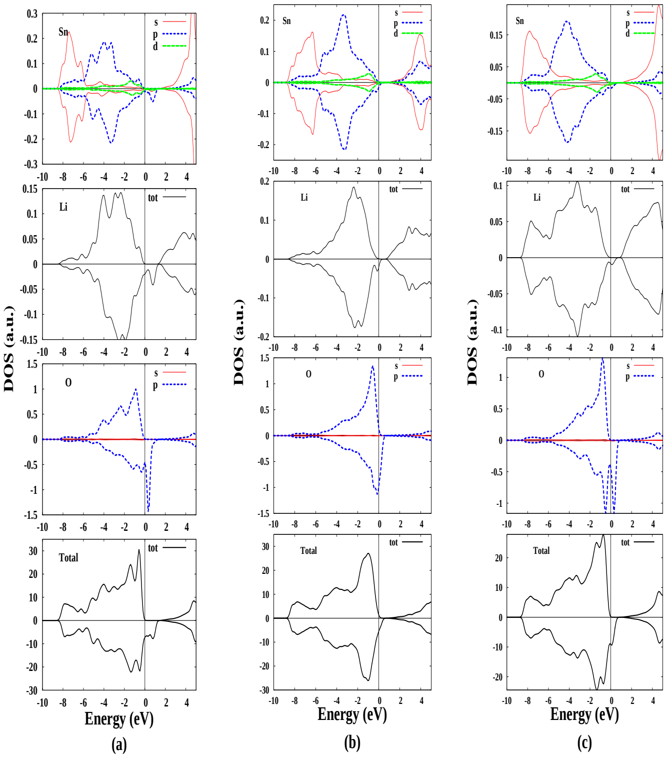

FIG. 5: (color online)The calculated total and partial density of states (DOS) of (a) $\mathrm{V_{Sn}}$+$\mathrm{Li_{Sn}}$, (b) $\mathrm{V_{Sn}}$+ $\mathrm{Li_O}$, and (c) $\mathrm{V_{Sn}}$+$\mathrm{Li_{int}}$ systems. Solid (red) and dashed (blue, green) lines represent *s* and *p*, *d* states, respectively. The bottom panel solid line represents the total DOS. The positive (negative) DOS shows majority (minority) spin states. The Fermi level (E_{F}) is set to zero.

It is very interesting that irrespective of the location of Li in Sn defective systems, it always reduces the formation energy of $\mathrm{V_{Sn}}$ and the systems remain magnetic. To further understand the electronic structure of $\mathrm{SnO_2}$ and the interaction of Li with native defects, we show the calculated total and atom projected densities of states in Fig. 5. The interaction of Li with native defects mainly affect the local DOS of the O atoms. Also, Li-O type of hybridizations can be seen around the Fermi levels. In all cases, the oxygen spin-up *p* orbitals are occupied whereas the spin-down *p* orbitals are partially occupied, similar to the DOS of $\mathrm{V_{Sn}}$.[7] It is noticeable that all the DOS figures show half metallic behavior except $\mathrm{V_{Sn}}$ + $\mathrm{Li_O}$ which anyhow has nearly half metallic behavior, mainly due to the *p* orbitals of the O atoms. It is also noticeable that when Li goes to an interstitial site in the presence of a Sn vacancy, the oxygen *p* orbitals are no longer degenerated at the Fermi level.

C. Interaction of O vacancies with Li

TABLE III: Formation energies (in units of eV) of systems $V_O + Li_{Sn}$, $V_O + Li_O$, and $V_O + Li_{int}$ calculated under equilibrium (E_{eq}), Sn-rich (E_{Sn}) and O-rich (E_O) conditions. The distance from V_O to Li_{Sn}, Li_O, and Li_{int} is $r - r_j$ (in units of Å). The last column lists the calculated magnetic moments (MM) per supercell (in units of μ_B). Values in brackets show the formation energies of the unrelaxed structures.

System	$r - r_j$	E_{eq}	E_{Sn}	E_O	MM
V_O		1.64(1.69)	1.64(1.69)	5.42(5.47)	0.00
$V_{Oj} + Li_{Sn}$					
$V_{O1} + Li_{Sn}$	2.04	-2.55(-0.07)	5.01(7.49)	1.23(3.71)	1.00
$V_{O2} + Li_{Sn}$	2.08	-2.34(-0.50)	5.22(7.06)	1.44(3.28)	1.00
$V_{O3} + Li_{Sn}$	4.71	-3.69(-2.11)	3.87(-2.11)	0.09(1.67)	1.00
$V_{O4} + Li_{Sn}$	5.71	-2.09(-2.69)	3.39(4.86)	-0.39(1.08)	1.00
$V_O + Li_{Oj}$					
$V_O + Li_{O1}$	2.94	0.15(3.48)	0.15(3.48)	3.93(7.27)	0.00
$V_O + Li_{O2}$	3.47	0.21(5.01)	0.21(5.01)	3.98(8.79)	0.00
$V_O + Li_{O3}$	5.15	0.30(3.80)	0.30(3.80)	4.08(7.59)	0.00
$V_O + Li_{int}$					
$V_O + Li_{int}$	3.48	-0.96(0.37)	-0.96(0.37)	1.36(4.16)	0.00

It is believed that Sn vacancies have higher formation energy as compared with O vacancies. Indeed, we found that the O vacancy has defect formation energy (1.64 eV) much smaller than that for the Sn vacancy. We therefore considered also the interactions of O vacancies with Li. First, we doped Li at the Sn site and varied the position of the O vacancy. The calculated defect formation energies are shown in Table (III). Interestingly, doping of Li at the Sn site appreciably reduced the defect formation energy of V_O. The defect complex $V_{O3} + Li_{Sn}$ has the lowest formation energy, -3.69 eV in equilibrium conditions. Such a favorable process implies that oxygen vacancies also promote magnetism in doped systems. We must stress that oxygen vacancies by itself are nonmagnetic[7], but however, become magnetic in the presence of Li_{Sn}, which is magnetic. Either Li_{Sn} or V_O have large defect formation energies, but the defect complex $V_O + Li_{Sn}$ has a lower energy than the individual defects. It is interesting to see that these defects complex always give magnetism with magnetic moments of 1.00 μ_B, no matter how far is V_O from Li_{Sn}. Such behavior is different from Co-doped SnO_2 where it has been shown that V_O quenches magnetism when Co_{Sn} is away from V_O.[39] On the other hand, Ni-doped SnO_2 does not show magnetism without V_O.[40] We therefore believe that Li-doped SnO_2 is another candidate material for spintronics. We also found that V_O and Li_O do not induce magnetism in SnO_2, as seen in Table (III), but the formation energy of this complex is always bigger than that of the $V_O + Li_{Sn}$ complex, excluding under Sn-rich conditions. There are some experimental reports which claim that oxygen vacancies are responsible for room temperature ferromagnetism in oxides[41] but to date, there are no experiments reports which show that a single neutral V_O is the main source of magnetism in SnO_2. Generally, it is believed that V_O promotes magnetism in doped SnO_2.[39,40] which is proven by our extensive calculations (see Table (III)). We also considered Li at different O sites in the presence of O vacancies but the calculated E_f show that these configurations are less stable than the $V_O + Li_{Sn}$ (excluding Sn-rich conditions).

Finally, the interaction of O vacancies with Li_{int} was also taken into account. The calculated E_f of $Li_{int}+V_O$ are given in Table (III) which shows that the behavior of $Li_{int}+V_O$ is quite different from $Li_{int}+V_{Sn}$. Li_{int} reduces the formation energy of V_{Sn}, but however Li_{int} does not decrease the formation energy of V_O. Also such kinds of defect complexes have zero magnetic moments. From Table (II) and Table (III), we can see that E_f can be reduced by Li, but at the same time thermodynamics also tell us that in the presence of a Sn vacancy the probable location of Li will be the O site where structural relaxation is also expected. On the other hand, Li prefers the Sn site rather than the O site, when the interactions of O vacancies with Li_O is considered.

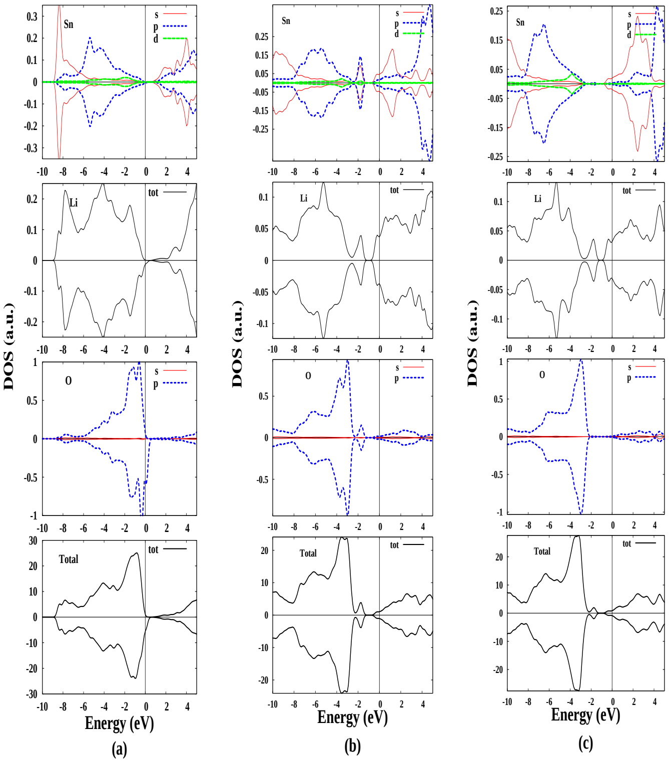

FIG. 6: (color online)The calculated total and partial density of states (DOS) of (a) V_O+Li_{Sn} (b) V_O+Li_O, and (c) V_O+Li_{int} systems. Solid (red) and dashed (blue, green) lines represent s and p, d states, respectively. The bottom panel solid line represents the total DOS. The positive (negative) DOS shows majority (minority) spin states. The Fermi level (E_F) is set to zero.

Before summarizing our work, the electronic structure of the above mentioned defect complexes will be presented. Figure 6(a) shows that the electronic structure is similar to $\mathrm{Li_{Sn}}$, i.e., the magnetism is mainly contributed by the O p orbitals and the Li-O type hybridization can also be seen near the Fermi level. No magnetism can be seen in Fig. 6(b) which represents the $\mathrm{V_O}$+$\mathrm{Li_O}$ defect system. The impurity peak around 2 eV below E_F is contributed by the Li atom. The conduction and valance bands are separated from each other and the Fermi level crosses the conduction band, which is mainly formed by Sn s and Li orbitals. This electronic structure indicates that Li in the $\mathrm{V_O}$ system will behave as an electron donor. The electronic structure of $\mathrm{V_O}$+$\mathrm{Li_{int}}$ [Fig. 6(c)] also shows nonmagnetic behavior. The O p orbitals are completely occupied and are far from E_F. The Li and Sn atoms occupy the conduction band, i.e., $\mathrm{V_O}$+$\mathrm{Li_{int}}$ is also a n type material. Comparing the DOS of the $\mathrm{Li_{int}}$ system with that of the $\mathrm{V_O}$+$\mathrm{Li_{int}}$, we see that $\mathrm{V_O}$ pushes the valance band of $\mathrm{Li_{int}}$ to lower energy states. From the given DOS in Figs. (2), (5), and (6), we may say that those systems in which E_F cuts the conduction bands, i.e., which behave as electron donors, do not show magnetism. This indicates that magnetism in $\mathrm{SnO_2}$ is mediated by holes and destroyed by electrons. Further experimental work is needed to validate our theoretical calculations.

IV. SUMMARY

We investigated the energetics and magnetism of Li-doped $\mathrm{SnO_2}$ systems with and without native defects using density functional theory (DFT). Lithium was doped at Sn, O, and interstitial sites and it was shown that it can induce magnetism in $\mathrm{SnO_2}$ when doped at the Sn site. No magnetism was found however when Li was doped at the O and interstitial sites. The defect formation energies showed that Li doped at the Sn site is more favorable than doped at the O site. We found that Li at the Sn site also shows a large magnetic moment ($3.00\mu_\mathrm{B}$), and the origin of magnetism was discussed in terms of electronic structures and spin densities. Native defects, Sn vacancy ($\mathrm{V_{Sn}}$) and O vacancy ($\mathrm{V_O}$), were also studied and it was observed that magnetic $\mathrm{V_{Sn}}$ has higher defect formation energy than non magnetic $\mathrm{V_O}$. To reduce the defect formation energies of these native defects, the interactions of Li with $\mathrm{V_{Sn}}$ and $\mathrm{V_O}$ were also studied. The calculated defect formation energies of these native defects were significantly decreased by Li. Our calculations showed that $\mathrm{V_O}$ helps to promote magnetism in Li doped $\mathrm{SnO_2}$, in agreement with general experimental speculations. Structural relaxations were shown to be important when the interactions of Li with $\mathrm{V_{Sn}}$ were considered. Comparison of our studied system with the previously synthesized systems was also discussed and it was concluded that Li doped $\mathrm{SnO_2}$ is another good candidate in the filed of magnetism.

Acknowledgments

We are grateful to S. K. Hasanain for useful discussions on the experimental realization of the studied systems. GR acknowledges the cluster facilities of NCP, Pakistan. VMGS thanks the Spanish Ministerio de Economía y Competitividad for a Ramón y Cajal fellowship (RYC-2010-06053).

---

* Electronic address: gulrahman@qau.edu.pk

[1] K. Ueda, H.Tabata, and T.Kawai, Appl. Phys. Lett. **79**, 988 (2001).
[2] K. Yang, R. Wu, L. Shen, Y. Ping Feng, Y. Dai, and B. Huang, Phys. Rev. B **81**, 125211 (2010).
[3] K. S. Yang, Y. Dai, and B. B. Huang, J. Chem. Phys. **10**, 2327 (2009).
[4] K. S. Yang, Y. Dai, B. B. Huang, and M. H. Whangbo, Appl. Phys. Lett.**93**, 132507 (2008).
[5] K. S. Yang, Y. Dai, B. B. Huang, and Y. P. Feng, Phys. Rev. B **81**, 033202 (2010).
[6] S. B. Ogale1, R. J. Choudhary, J. P. Buban, S. E. Lofland, S. R. Shinde, S. N. Kale, V. N. Kulkarni, J. Higgins, C. Lanci, J. R. Simpson, N. D. Browning, S. Das Sarma, H. D. Drew, R. L. Greene, and T. Venkatesan, Phys. Rev. Lett. **91**, 077205 (2003).
[7] G. Rahman, Víctor M. García-Suárez, and S. C. Hong, Phys. Rev. B **78**, 184404 (2008).
[8] M. Khalid, M. Ziese, A. Setzer, P. Esquinazi, M. Lorenz, H. Hochmuth, M. Grundmann, D. Spemann, T. Butz, G. Brauer, W. Anwand, G. Fischer, W. A. Adeagbo, W. Hergert, and A. Ernst, Phy. Rev. B **80**, 035331 (2009).
[9] D. Kim, J. Hong, Y. Ran Park and K. Joo Kim, J. Phys.: Condens. Matter **21**, 195405 (2009).
[10] F. Máca, J. Kudrnovský, V. Drchal, and Georges Bouzerar, Appl. Phys. Lett. **92**, 212503 (2008).
[11] L. X. Guan, J. G. Tao, C. H. A. Huan, J. L. Kuo, and L. Wang, J. Appl. Phys. **108**, 093911 (2010).
[12] V. Fernandes, P. Schio, A. J A de Oliveira, W. A. Ortiz, P. Fichtner, L. Amaral, I. L. Graff, J. Varalda, N. Mattoso, W.H. Schreiner and D. H. Mosca, J. Phys.: Condens. Matter **22** 216004 (2010).
[13] J. Osorio-Guillén, S. Lany, S. V. Barabash, and A. Zunger, Phy. Rev. B **75**, 184421 (2007).
[14] S. K. Srivastava, P. Lejay, B. Barbara, S. Pailhés, V. Madigou, and G. Bouzerar, Phys. Rev. B **82**, 193203 (2010).
[15] W. Zhi Xiao, L. Ling Wang, L. Xu, Q. Wan, and Zou, Solid State Communications **149**, 1304-1307 (2009).
[16] C. Wen Zhang, and S. shen Yan, Appl. Phys. Lett. **95**, 232108 (2009).
[17] G. Rahman and V. M. García-Suárez, Appl. Phys. Lett. **96**, 052508(2010).
[18] N. H. Hong, J. H. Song, A. T. Raghavender, T. Asaeda,

and M. Kurisu, Appl. Phys. Lett. **99**, 052505 (2011).

[19] N. Hoa Hong, J. H. Song, A. T. Raghavender, T. Asaeda, and M. Kurisu, Apl. Phys. Lett **99**, 052505 (2011).

[20] J. B. Yi, C. C. Lim, G. Z. Xing, H. M. Fan, L. H. Van, S. L. Huang, K. S. Yang, X. L. Huang, X. B. Qin, B. Y. Wang, T. Wu, L. Wang, H. T. Zhang, X. Y. Gao, T. Liu, A. T. S. Wee, Y. P. Feng, and J. Ding, Phys. Rev. Lett. **104**, 137201 (2010).

[21] S. Ghosh, G. G. Khan, and K. Mandal, Appl Mater Interfaces. **4**, 2048 (2012).

[22] G. S. Chang, J. Forrest, E. Z. Kurmaev, A. N. Morozovska, M. D. Glinchuk, J. A. McLeod, A. Moewes, T. P. Surkova, and N. Hoa Hong, Phys. Rev. B **85**, 165319 (2012).

[23] V. Golovanov, N. Ozcan, M. Viitala, T. T. Rantala and J. Vaara, *NATO Science for Peace and Security Series B: Physics and Biophysics, 2012, Part 2, 315*

[24] C. Wang, Q. Wu, H. L. Ge, T. Shang, and J. Z. Jiang Nanotechnology **23**, 075704(2012).

[25] C. Klyc and A. Zunger, Phys. Rev. Lett. **88**, 095501 (2002).

[26] C. D. Pemmaraju and S. Sanvito, Phys. Rev. Lett. **94**, 217205(2005).

[27] W. Wei, Y. Dai, M. Guo, K. Lai, and B. Huang, J. Appl. Phys. **108**, 093901 (2010).

[28] W. Wei,Y. Dai, M. Guo,Z. Zhang,and B. Huang, J. Solid State Chem **183**, 3073-3077 (2010).

[29] M. Mehdi, B. Mohagheghi, and M. Shokooh-Saremi, Semicond. Sci. Technol. **19**, 764 (2004).

[30] J. Haines and J. M. Léger, Phys. Rev. B **55**, 11144 (1997), A. A. Bolzan, C. Fong, B. J. Kennedy, and C. J. Howard, Acta Crystallogr. B **53**, 373 (1997).

[31] P. Hohenberg and W. Kohn, Phys. Rev. **136**, B846 (1964).

[32] J. M. Soler et al J. Phys.Condens.: Matter **14**, 2745 (2002).

[33] J. P. Perdew and A. Zunger, Phys. Rev. B **23**, 5048 (1981).

[34] D. R. Hamann , M. Schlúter and C. Chiang, Phys. Rev. Lett. **43**, 1494 (1979).

[35] L. Kleinman and D. M. Bylander, Phys. Rev. Lett. **48**, 1425 (1982).

[36] W. H. Press, B. P. Flannery, S. A. Teukolsky, W. T. Vetterling, New Numerical Recipes, Cambridge University Press, New York, 1986.

[37] A. F. Kohan, G. Ceder, and D. Morgan, Phys. Rev. B **61**, 15019 (2000).

[38] J. M. Themlin, R. Sporken, J. Darville, R. Caudano, and J. M. Gilles, Phys.Rev. B **42**, 11915 (1990).

[39] C. Zhang and S. Yan, J. Appl. Phys. **106**, 063709 (2009).

[40] H. Wang, Y. Yan, X. Du, X. Liu, K. Li, and H. Jin, J. Appl. Phys. **107**, 103923 (2010).

[41] N. H. Hong, J. Sakai, W. Prellier, and A. Hassini, J. Phys.: Condens.Matter **17**, 1697 (2005).